*Original Article*

# CELLULAR COMPONENTS AND THEIR CORRELATIONS IN THE SUBCHONDRAL BONE PLATE AND CANCELLOUS BONE OF PATIENTS WITH KNEE OSTEOARTHRITIS

Xiaobo Zhu[1,2,3], Mingde Cao[1,2,3], Chen Hu[4,5], Kevin Ki-Wai Ho[2,3], Michael Tim-Yun Ong[2,3], Wenqing Xie[6], Ziyang Xu[1,3,7], Wenfeng Xiao[6], Patrick Shu-Hang Yung[1,2,3], Yusheng Li[6], Changjun Li[4,5,*], and Yangzi Jiang[1,2,3,7,8,*]

[1]Institute for Tissue Engineering and Regenerative Medicine, The Chinese University of Hong Kong, Hong Kong SAR, China
[2]Department of Orthopaedics & Traumatology, Faculty of Medicine, The Chinese University of Hong Kong, Hong Kong SAR, China
[3]Center for Neuromusculoskeletal Restorative Medicine (CNRM), The Chinese University of Hong Kong, Hong Kong SAR, China
[4]National Clinical Research Center for Geriatric Disorders, Xiangya Hospital, Central South University, 410008 Hunan, Changsha, China
[5]Department of Endocrinology, Xiangya Hospital, Central South University, 410008 Hunan, Changsha, China
[6]Department of Orthopaedic, Xiangya Hospital, Central South University, 410008 Hunan, Changsha, China
[7]School of Biomedical Sciences, The Chinese University of Hong Kong, Hong Kong SAR, China
[8]Key Laboratory for Regenerative Medicine, Ministry of Education, School of Biomedical Sciences, Faculty of Medicine, The Chinese University of Hong Kong, Hong Kong SAR, China

**Abstract**

**Objective**: The load-bearing structures of the subchondral bone undergo alterations in osteoarthritis (OA) joints and exhibit distinct bone remodelling properties. This study examined the pathological features and cellular components of the subchondral bone plate (SCBP) and subchondral cancellous bone (SCCB) in OA-affected regions of human knee joints. **Methods**: Tibial plateaus were obtained from patients with varus knee OA (n = 42; women: n = 22, aged 57–87 years; men: n = 20, aged 59–82 years). Osteochondral specimens were collected from OA lesion sites in the medial compartment (OA region) and paired control sites in the lateral compartment (C region). Bone mineral density (BMD) was evaluated using micro-computed tomography, osterix$^+$ osteoprogenitors, cathepsin K (CTSK)$^+$ osteoclasts, and F4/80$^+$ macrophages were quantified by immunohistochemistry, and correlations between cellular components were analysed by sex and region. **Results**: The OA SCBP had a significantly higher BMD than did the C region. In male patients, more F4/80$^+$ macrophages were present in the SCBP C region than in the OA region. Female OA SCCB samples showed an increased number of CTSK$^+$ osteoclasts. In both sexes, compared with the C region, the OA SCCB contained more CTSK$^+$ osteoclasts and macrophages. Positive correlations between macrophage and osteoprogenitor densities were observed in most subchondral bone regions, except in male OA samples. **Conclusions**: Region-specific differences in cellular components were identified in the OA subchondral bone. Asynchronous remodelling responses were noted between the SCBP and SCCB. These findings provide detailed insights into OA pathology and can inform future therapeutic strategies.

**Keywords:** Macrophage, sclerosis, subchondral bone plate, tibial plateau, trabeculae, osteoclast.

***Address for correspondence**: Yangzi Jiang, Institute for Tissue Engineering and Regenerative Medicine, The Chinese University of Hong Kong, Hong Kong SAR, China; Department of Orthopaedics & Traumatology, Faculty of Medicine, The Chinese University of Hong Kong, Hong Kong SAR, China; Center for Neuromusculoskeletal Restorative Medicine (CNRM), The Chinese University of Hong Kong, Hong Kong SAR, China; School of Biomedical Sciences, The Chinese University of Hong Kong, Hong Kong SAR, China; Key Laboratory for Regenerative Medicine, Ministry of Education, School of Biomedical Sciences, Faculty of Medicine, The Chinese University of Hong Kong, Hong Kong SAR, China. E-mail: yangzjiang21@cuhk.edu.hk; Changjun Li, Department of Endocrinology, Xiangya Hospital, Central South University, 410008 Hunan, Changsha, China; National Clinical Research Center for Geriatric Disorders, Xiangya Hospital, Central South University, 410008 Hunan, Changsha, China. E-mail: lichangjun@csu.edu.cn.

## Introduction

The subchondral bone provides structural support to the articular cartilage in the joint and undergoes active remodelling in response to mechanical loading. The subchondral bone plate (SCBP) is cortical-like, whereas the underlying subchondral cancellous bone (SCCB) is composed of trabeculae [1,2]. Clinical radiographs reveal various dynamic changes [3,4] and pathological alterations [5,6] in the subchondral bone of patients with osteoarthritis (OA). The prevalence of early knee OA is high among patients who have sustained anterior cruciate ligament (ACL) injury and undergone reconstruction, which is likely to be due to altered mechanical loading patterns after surgery [7]. Knees reconstructed after ACL injury exhibit a thicker SCBP in the femoral posterior and central lateral regions [8,9] and decreased bone mineral density (BMD) in the subchondral cancellous region compared with healthy and contralateral knees [9,10]. In patients with early-stage OA (Kellgren–Lawrence grade 1 or 2; KL 1/2), Bolbos *et al*. [10] observed subchondral bone changes similar to those in ACL-reconstructed knees and decreased BMD in the subchondral cancellous region compared with patients without OA. In their 2021 study, Li *et al*. [11] reported that in patients with end-stage OA, the sclerotic subchondral bone was present in both the SCBP and cancellous regions. Although numerous animal studies have elucidated the structural and molecular changes in the subchondral bone during OA [12,13], limited attention has been given to the asynchronous responses of the SCBP and SCCB in human OA joints, particularly in cases with disorganised load-bearing zones. Because the human subchondral bone comprises distinct subregions, namely the SCBP, SCCB, and load-bearing and non-load-bearing OA areas, further investigation is warranted to determine the spatial differences in these regions [14,15] and clarify their key cellular features in OA.

Bone remodelling follows Wolff's law, where osteoclastogenesis and osteogenesis are spatially and temporally coordinated [16]. During a bone remodelling cycle, osteoclasts (cathepsin $K^+$, $CTSK^+$ cells) resorb the bone matrix and create a microenvironment that supports bone marrow mesenchymal stem cells, inducing their differentiation into osteoprogenitor cells ($Osterix^+$ cells) and facilitating subsequent bone formation [13,17]. $Osterix^+$ and $CTSK^+$ cells reflect the dynamic processes of bone formation and resorption, whereas the biological functions of macrophages in bone remodelling remain unclear. A recent study reported that in addition to osteoclasts, the bone also contains a population of tissue-resident macrophages [18]. These cells are mainly located in the endosteal and periosteal areas and are positive for F4/80 [18]. $F4/80^+$ bone-resident macrophages support osteoblast differentiation and mineralisation in vitro, promote both endochondral and intramembranous ossification during fracture healing [19], and contribute to endplate osteosclerosis in Modic changes in the degenerative spine [20]. These cells also supported bone resorption in a postmenopausal osteoporosis mouse model [21]. Taken together, osteoprogenitors, osteoclasts, and tissue-resident macrophages are the major responders in knee OA in the subchondral bone plate and cancellous bone.

Cells within the subchondral bone may respond differently to mechanical stimuli during bone remodelling. For instance, macrophages in the bone are likely to respond to mechanical loading. In an in vitro study, mechanical force (5% stretch for 12 hours) induced M2 polarisation of the RAW 264.7 macrophage cell line, altered its cytokine secretion profile, and enhanced the osteogenic differentiation of bone marrow mesenchymal stem cells [22]. Similar effects were observed in vivo, where daily compressive loading of 2–12 N (360 cycles, 3 times per week for 4 weeks) increased the number of in situ periosteal $CD68^+F4/80^+$ macrophages and enhanced cortical bone formation in a murine tibial loading model [23]. A subsequent mechanistic study revealed that periosteal $CD68^+F4/80^+$ macrophages promoted bone formation by secreting transforming growth factor-$\beta$1 in response to daily compressive loading [23]. Like macrophages, osteoclasts are sensitive to mechanical stimuli. In one study, osteoclastogenesis was observed in the maxillary right molars of rats after direct cyclic mechanical loading. Specifically, cyclic loading of 20, 30, or 40 N (100%, 150%, or 200% of the masticatory loading force) at 5.8 Hz for 30 min daily over 7 days was applied in a rat periodontal loading model. Excessive cyclic loading at 30–40 N significantly increased the number of osteoclasts in the periodontal tissue [24]. In addition to direct mechanical loading, osteoclasts are sensitive to extracellular matrix stiffness. Wang *et al*. [25] cultured osteoclast lineage cells on hydrogels spanning a physiological stiffness range (2.43–68.2 kPa) and found that increasing matrix stiffness markedly promoted osteoclastogenesis, with the number of TRAP-positive multinucleated osteoclasts rising and then plateauing around 29.4 kPa, while osteoclast size and bone-resorptive activity continued to increase at higher stiffness. Notably, an intermediate "vessel-like" stiffness (~17–45 kPa) maximized the accumulation of TRAP-positive preosteoclasts without further increasing osteoclast number. Collectively, these findings indicate that the bioactivity of bone-resident macrophages and osteoclasts can be regulated by mechanical loading conditions. Notably, in the carpal bones of racehorses with post-traumatic OA, osteoclasts predominantly accumulated in the SCBP at high load-bearing sites rather than in the SCCB [26], suggesting a region-specific bone remodelling response to mechanical loading. Recent studies have identified similar region-specific adaptations in the subchondral bone of human varus OA knee joints [27–29]. Areas closer to the mechanical axis consistently exhibited thinner cartilage, an increased SCBP thickness, and a higher bone volume to tissue volume ratio (BV/TV). These findings suggest that subchondral bone sclerosis is most pronounced

near the load-bearing centre of the tibial plateau [27]. In varus OA knees, malalignment-induced overload leads to progressive sclerosis in the medial compartment, and the infiltration of $CD68^+$ macrophages has been observed in the sclerotic regions of arthroplasty specimens [28,29]. Collectively, these findings indicate that osteoclasts and tissue-resident macrophages actively contribute to subchondral bone remodelling in OA. However, the region-specific distribution patterns and mechanical response characteristics of osteoclasts and $F4/80^+$ tissue-resident macrophages in the OA subchondral bone remain poorly characterised.

In addition to responses to mechanical loading, OA-related alterations in the subchondral bone may exhibit sexual dimorphism, potentially due to the protective effects of oestrogen on the bone and cartilage. Oestrogen deficiency is a well-established risk factor for OA in post-menopausal women [30]. Mechanistically, oestrogen exerts a bone-protective effect by enhancing osteoblast activity, slowing subchondral bone degradation, and promoting physiological remodelling in OA-affected joints [31,32]. However, most current evidence is derived from animal studies, with limited validation in human clinical samples.

This study examined pathological changes in the subchondral bone of patients with OA, focusing on the SCBP and SCCB regions in 42 human tibial plateaus. In addition, the corresponding cellular activities of osteoclasts and tissue-resident macrophages were evaluated. The hypothesis is that bone remodelling-associated cells (osteoprogenitors, osteoclasts, and macrophages) exhibit specific cellular profiles across different load-bearing regions of the OA subchondral bone (SCBP and SCCB) and potential sex-specific variations in their distribution and activity.

## Materials and Methods

*Study participants*

Tibial plateaus were collected from patients undergoing total knee arthroplasty during 2020 August to 2022 November, and written informed consent was obtained from each participant. The study protocol was approved by the Human Research Ethics Committees of the local administrative parties. Patients receiving anti-resorptive drugs, corticosteroids (via either systemic administration or intra-articular injection), or hormone replacement therapy that could affect bone metabolism were excluded. A total of 42 patients were included (20 men, aged 57–87 years; mean age: 71.0 years and 22 women, aged 59–82 years; mean age: 69.4 years), all of whom had radiographic evidence of KL grade 3 or 4 OA. The detailed description of KL grade system is present in **Supplementary Material Table 4**. All patients presented with varus deformity, as determined by measurements of the hip–knee–ankle (HKA) angle [33] and the medial proximal tibial angle (MPTA) on radiographs (mean HKA: 169.7° ± 5.9°; mean MPTA: 88.2° ± 4.6°.

*Regional tissue preparation and micro-computed tomography quantification*

All specimens were transferred from the operating room to the laboratory immediately after dissection, fixed in 4% paraformaldehyde at 4°C for 48 hours, and trimmed into osteochondral tissue blocks. Full-thickness tissue blocks (1.5 cm × 0.5 cm) were collected from remote control sites (C region) in the lateral tibial plateau and from OA lesion sites (OA region) in the medial tibial plateau of the same donor. Tissue blocks obtained from the C region had visually intact cartilage, whereas those from the load-bearing OA region showed severe cartilage erosion, with exposed subchondral bone displaying an osteosclerotic phenotype. A total of 20 paired tissue blocks obtained from 10 biological donors (5 men and 5 women) were randomly selected and subjected to micro-computed tomography ($\mu$CT) scanning (Scanco 35, Switzerland). The $\mu$CT scanner was operated under the following parameters: voltage, 70 kVp; current, 140 $\mu$A; resolution, 10 $\mu$m/pixel. For image reconstruction and data analysis, 50 slices were contoured and evaluated using a global threshold of 250, covering the full thickness of the subchondral bone below the articular cartilage (Fig.1). All images were smoothed using a Gaussian filter (sigma: 0.8, support: 1.0). The following parameters were analysed: trabecular number, trabecular thickness, trabecular separation, BV/TV, and BMD.

*Histology and OARSI scores of the articular cartilage*

After $\mu$CT scanning, the tissue blocks were decalcified for histological analysis (SBS Core-Lab, The Chinese University of Hong Kong). Briefly, specimens were decalcified in 0.5 M $Na_2$-EDTA solution (pH 7.35–7.45, refreshed daily) for 2 weeks, embedded in paraffin, and sectioned serially at a thickness of 5 $\mu$m. The sections were stained with haematoxylin and eosin and Safranin O/fast green. Images were captured using a light microscope (Leica DM5500, Germany) [34]. The pathological severity of OA was evaluated and scored using the conventional Osteoarthritis Research Society International (OARSI) scoring method [35], which examines articular cartilage degeneration, cartilage thickness, cartilage lesions, and chondrocyte hypertrophy.

*Immunohistochemistry*

All samples were subjected to immunohistochemical analysis by us. Cellular markers for osteoclasts ($CTSK^+$), osteoprogenitors ($Osterix^+$), and resident macrophages ($F4/80^+$) were detected using immunohistochemistry. Deparaffinised sections were initially incubated with a primary antibody, namely anti-Osterix (Abcam, Cambridge, MA, USA, ab22552; 1:300), anti-cathepsin K (Abcam, Cambridge, MA, USA, ab19027; 1:500), or anti-F4/80 (Abcam, Cambridge, MA, USA, ab254293; 1:50), overnight at 4 °C and then with a secondary antibody (Proteintech, Wuhan, China, SA0001-2, 1:200) for 1 hour at room tem-

perature. Positive staining was visualised using a 3,3′-diaminobenzidine tetrahydrochloride horseradish peroxidase system development kit (Thermo Fisher Scientific, Waltham, MA, USA, TA-060-QHDX) and counterstained with haematoxylin. Cell density and positive cell counts were quantified using ImageJ software (National Institutes of Health, Bethesda, MD, USA) as described previously [36]. Based on structural characteristics, cell density in the SCBP was calculated as the number of positively stained cells per $mm^2$ bone marrow cavity area, whereas in the SCCB, density was calculated as the number of positively stained cells per mm of bone surface (see details for ROI selection and method for quantification in **Supplementary Material Fig.1**). Positively stained cells in each region of interest (ROI) were counted from images captured at 20× magnification and quantified using Image J (National Institutes of Health). For each SCBP sample, the observer randomly analysed three bone marrow cavities and calculated the average value as the representative cell density. The SCBP samples containing fewer than three bone marrow cavities were excluded from the quantification. The ratios of cellular components were determined as the proportion of each specific cell type (cell density of interest / ($F4/80^+$ + $Osterix^+$ + $CTSK^+$ cell densities)), and correlations between osteoprogenitors and macrophages in different regions were further analysed.

### *Statistical analysis*

GraphPad Prism 7.0 (GraphPad Software, La Jolla, CA, USA) and SPSS 21.0 (IBM Corp, Armonk, NY, USA) were used for data analysis. Ten patients (5 men and 5 women) were randomly selected from the cohort for $\mu$CT analysis. The sample size for the $\mu$CT experiment was estimated using G*Power software (version 3.1.2, Franz Faul, Germany) based on previous studies [12,36] and preliminary data. The calculation was performed using an alpha level of 0.05 and a desired statistical power of 80%. The $\mu$CT analysis was mainly performed to quantify well-established OA-related pathological changes in the subchondral bone, which have been extensively reported in previous studies with larger sample sizes [12]. The normality of data distribution and homogeneity of variances were determined using the Shapiro–Wilk test and Levene's test, respectively. A paired Student's t test was used to compare the results of $\mu$CT analysis between two groups. For other assays, the Wilcoxon signed-rank test was used when data were non-normally distributed or exhibited a significant homogeneity of variances in histological measurements. Spearman's rank correlation was performed to determine relationships among histological parameters, with both the correlation coefficient r and p value reported. All results are presented as the mean ± standard deviation. A $p$ value of $< 0.05$ was considered statistically significant. Detailed statistical methods used for each experiment are listed in **Supplementary Material Table 2**.

**Table 1. Characteristics of patients.**

| Characteristics | Findings |
|---|---|
| Age (years), mean ± SD | 70.2 ± 6.6 |
| BMI (body weight/height$^2$, kg/m$^2$), mean ± SD | 26.2 ± 3.5 |
| Sex (M/F) | 42 (20/22) |
| Kellgren–Lawrence grade, mean ± SD | 3.6 ± 0.5 |
| Lower extremity varus (HKA), mean ± SD | 169.7° ± 5.9° |
| Tibial plateau inclination (MPTA), mean ± SD | 88.2° ± 4.6° |
| OARSI score (lateral), mean ± SD | 1.7 ± 0.9 |
| OARSI score (medial), mean ± SD | 19.9 ± 4.6 |

SD: standard deviation; BMI: body mass index; HKA: hip–knee–angle; MPTA: medial proximal tibial angle; OARSI: Osteoarthritis Research Society International.

**Table 2. Characteristics of the cartilage in different regions.**

| | OARSI scores | | |
|---|---|---|---|
| | Men (n = 20) | Women (n = 22) | Total (n = 42) |
| C | 1.6 ± 0.6 | 1.8 ± 1.0 | 1.7 ± 0.9 |
| OA | 19.3 ± 4.8 | 19.6 ± 5.3 | 19.4 ± 5.0 |

OARSI, Osteoarthritis Research Society International; C, remote control sites located in the lateral tibial plateaus with a grossly normal cartilage; OA, OA lesion sites in the medial tibial plateaus.

## Results

### *Paired osteochondral tissue from C and OA regions and OARSI scores of the cartilage*

Forty-two tibial plateaus were collected from patients undergoing total knee arthroplasty, and paired osteochondral tissues were collected from the C and OA regions of each tibial plateau. Detailed information on all donors is presented in Table 1 and **Supplementary Material Table 1**. No statistically significant differences in age, body mass index (BMI), hypertension, and diabetes were observed between male and female donors (**Supplementary Material Table 3**).

The C region, located on the lateral side of the tibial plateau (Fig. 1**a**, box 1), and the degenerated region on the medial side is included as the OA region (Fig. 1**a**, box 2). The cartilage in the C region was nearly intact, with only minor fibrillations (Fig. 1**a** and **b**), whereas the cartilage in the OA region was severely damaged and ulcerated (Fig. 1**a** and **b**). The OARSI scores of the articular cartilage in the paired osteochondral tissues are presented in Table 2. The OA region had a significantly higher OARSI score than did the C region (OA vs. C: 19.4 ± 5.0 vs. 1.7 ± 0.9, $p < 0.01$).

### *Microstructure and BMD in the SCBP and SCCB*

To characterise subchondral bone tissues in the C and OA regions from male and female donors, the microstructure and BMD of the paired tissue blocks in the SCBP (Fig. 1**c**, ROI 1, red box; Fig. 1**d**, upper yellow box) and SCCB (Fig. 1**c**, ROI 2, blue box; Fig. 1**d**, downward red box) were evaluated using $\mu$CT. Twenty tissue blocks from 10

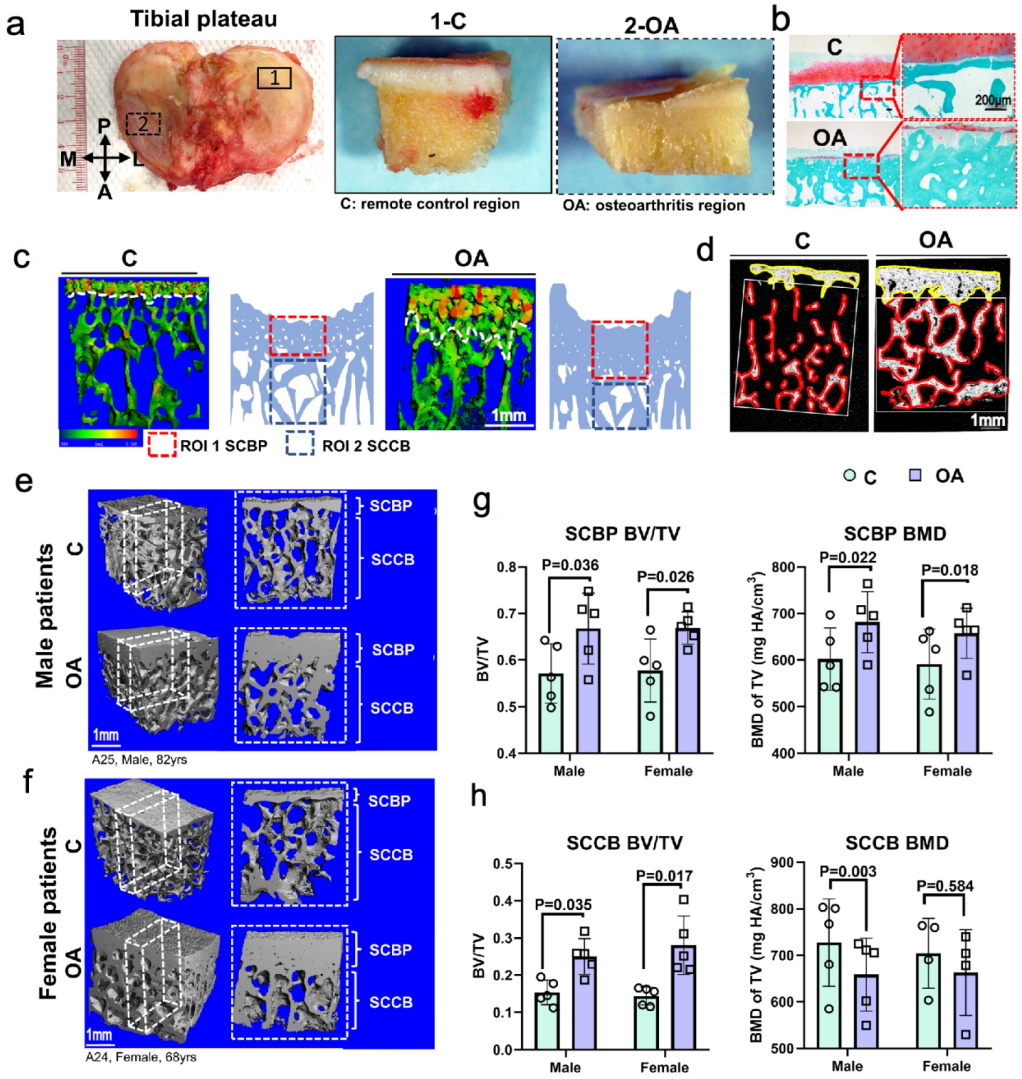


**Fig. 1. Paired osteochondral tissue from remote control regions (C) and regions with OA lesions harvested from human tibial plateaus after arthroplasty.** (**a**) Gross appearance of tibial plateaus from patients with OA. The image is from a 73-year-old male patient (patient number: A33). Box 1: C region; Box 2: OA region. Right panel: gross appearance of osteochondral specimens and articular surfaces trimmed from the C and OA regions. P: posterior; A: anterior; M: medial; L: lateral. (**b**) Representative Safranin O/fast green-stained images of C and OA regions of human subchondral bone tissues. Cartilage erosions and complete loss of Safranin O/fast green staining are observed in the OA region (lower panel). The OA region shows more bone structures compared with the C region. Magnified images display the SCBP and SCCB structures (dashed boxes). Scale bars = 200 $\mu$m. (**c**) Representative 3D $\mu$CT images of the subchondral bone from the C region (left panel) and OA region (right panel). ROI 1: red box, subchondral bone plate (SCBP); ROI 2: blue box, subchondral cancellous bone (SCCB). The grey–blue panels illustrate schematic diagrams of the human SCBP and SCCB. Scale bar = 1 mm. The white dotted line indicates the interface between the SCBP and SCCB; the red dotted line marks the SCBP; the blue dotted line marks the SCCB. (**d**) Segmentation of the SCBP (highlighted in yellow) and SCCB (highlighted in red) in $\mu$CT analysis. Scale bar = 1 mm. (**e–f**) 3D reconstruction of the tibial subchondral bone from the C and OA regions of a male patient with OA (e; patient number: A25, 82 years old) and a female patient with OA (f; patient number: A24, 68 years old). Scale bar = 1 mm. (**g–h**) Quantitative analysis of the ratio of bone volume to tissue volume (BV/TV, left panels) and bone mineral density (BMD, mg HA/cm$^3$, right panels) of the SCBP (**g**), and SCCB (**h**) from male and female donors (n = 5 per group). Statistical analysis between the C and OA regions from the same patient was performed using a paired *t* test. Data are presented as the mean ± SD. $p < 0.05$. C, remote control sites located in the lateral tibial plateaus with a grossly normal cartilage; OA, OA lesion sites in the medial tibial plateau; SCBP, subchondral bone plate; SCCB, subchondral cancellous bone; ROI, region of interest; BMD, bone mineral density; BV/TV, ratio of bone volume to tissue volume.

patients (n = 10 patients, 20 paired tissue blocks, paired OA and control regions, 5 men and 5 women) were subjected to $\mu$CT scanning. Quantitative $\mu$CT results for the SCBP and SCCB in the C and OA regions, stratified by sex, are presented in Fig. 1**e–h** and Table 3.

Overall, the OA region had a thickened SCBP. The BV/TV and BMD were significantly higher in the OA region than in the C region (OA vs. C: BMD, 669.5 ± 55.0 vs. 596.8 ± 63.8 mg HA/cm$^3$, $p < 0.001$; BV/TV, 0.67 ± 0.05 vs. 0.57 ± 0.06, $p < 0.001$). The SCCB in the OA region had a higher bone volume fraction than that in the C region (OA vs. C: BV/TV, 0.27 ± 0.06 vs. 0.15 ± 0.03, $p < 0.001$). In male donors, the SCCB of OA osteochondral blocks had a significantly lower BMD than that of the C region (male SCCB, OA vs. C: 658.6 ± 70.3 vs. 727.4 ± 84.0 mg HA/cm$^3$, $p = 0.001$). This trend was not statistically significant among female donors (Fig. 1**g–h**, Table 3). No significant differences in BMD were observed between sexes in either the SCBP or SCCB. Detailed $\mu$CT results and corresponding statistical analysis findings are presented in Table 3.

When data were stratified by sex, in the SCBP, a higher abundance of F4/80$^+$ macrophages was observed in the bone marrow cavities of the C region than in those of the OA region in male donors among all cells (OA vs. C: 425.4 ± 428.2 vs. 763.2 ± 617.3 cells/mm$^2$, n = 15, $p = 0.014$, Fig. 2**a–e**). In the SCCB of male donors, most cells were attached to the bone-lining surfaces (Fig. 3**a, e, f** and **j**), and F4/80$^+$ macrophages were more abundant in the OA region than in the C region among all cells (OA vs. C: 4.7 ± 3.3 vs. 2.3 ± 2.6 cells/mm, n = 18, $p < 0.001$; Fig. 3**a–e**). The same trend was observed for CTSK$^+$ osteoclasts (male SCCB, OA vs. C: 4.4 ± 3.2 vs. 1.5 ± 1.2 cells/mm, n = 18, $p < 0.001$; Table 4, Fig. 3**d** and **e**. In contrast, no significant difference in F4/80$^+$ macrophage distribution was observed between the C and OA regions in female donors either in the SCBP or SCCB (Table 4, Fig. 2**f, g, j**; Fig. 3**g** and **h**). Notably, in both male and female donors, CTSK$^+$ osteoclasts were more abundant in the OA region than in the C region in the SCCB but not in the SCBP (female SCCB, OA vs. C: 4.9 ± 4.7 vs. 1.7 ± 3.2 cells/mm, n = 22, $p = 0.006$, Fig. 3**i** and **j**; SCBP, OA vs. C: 262.3 ± 269.9 vs. 407.9 ± 674.9 cells/mm$^2$, n = 14, $p = 0.377$; Table 4, Fig. 2**i** and **j**).

### *Cellular components and their correlations in different regions of the OA subchondral bone*

Correlation analyses between cellular components were conducted using the same sample subsets described in table 4 (SCBP: n = 29; SCCB: n = 40), ensuring consistency across all statistical evaluations. The observed region-specific differences in cellular components were consistent with the pathological features of the articular cartilage and microstructural characteristics of the subchondral bone. The proportions of Osterix$^+$ osteoprogenitors, F4/80$^+$ resident macrophages, and CTSK$^+$ osteoclasts in the C and OA region are summarised in Fig. 4**a**, 4**b**, and 4**g**. In male patients, a greater number of macrophages were observed in the C region of the SCBP, whereas the SCCB contained higher numbers of both macrophages and osteoclasts in the OA region. These cellular alterations are presented in Fig. 4**g**.

In both male and female patients, positive correlations were observed between macrophages and osteoprogenitors with respect to their distribution and density (Fig. 4**c**–**f**). The densities of macrophages and osteoprogenitors were positively correlated in the C region of the SCBP (r = 0.771, $p = 0.002$; Fig. 4**c**), OA region of the SCBP (r = 0.873, $p < 0.001$; Fig. 4**d**), C region of the SCCB (r = 0.781, $p < 0.001$; Fig. 4**e**), and OA region of the SCCB (r = 0.821, $p < 0.001$; Fig. 4**f**) in female patients, and in the C region of the SCBP (r = 0.661, $p = 0.009$; Fig. 4**c**) and C region of the SCCB (r = 0.680, $p = 0.002$; Fig. 4**e**) in male patients.

## Discussion

In the present study, OA-related changes in the subchondral bone were examined using 42 zonally paired clinical samples (control and OA-affected areas). The findings revealed region-specific differences in cellular components, specifically among tissue-resident macrophages and osteoclasts in the SCBP and SCCB regions. The enrichment of F4/80$^+$ resident macrophages and osteoprogenitors in the male control SCBP and the positive correlation between these tissue-resident macrophages and osteoprogenitors (Fig. 4**c**, **e**) suggest that tissue-resident macrophages support bone formation in the OA subchondral bone. This finding is consistent with that of a previous study demonstrating that bone-resident macrophages support endochondral and intramembranous ossification during fracture healing [19]. In addition, a positive correlation between tissue-resident macrophages and osteoprogenitors was observed in the female OA subchondral bone (SCBP and SCCB) but not in the male OA subchondral bone (SCBP and SCCB; Fig.4**d**, **f**), suggesting sex-specific differences in subchondral bone remodelling patterns in OA.

In the data obtained from OA tibial plateaus, both bone volume and BMD were higher in all samples from the OA region of the SCBP. At the cellular level, fewer F4/80$^+$ resident macrophages were found in the male OA SCBP than in the control SCBP (Table 4), suggesting a loss of homeostatic balance in this region. A similar trend was noted among female donors, although the difference did not reach statistical significance. To obtain more precise measurements of the SCCB region, $\mu$CT analysis was performed [12] in which the volume of bone marrow cavities was excluded and only subchondral bone tissues were analysed (Fig. 1**d**). These data indicated that in male patients, the SCCB under the OA region had a higher bone volume but a lower BMD. Similar findings have been reported in

**Table 3. $\mu$CT parameters in different regions of interest and between sexes.**

| Grouping | Measurement | Men (n = 5) | | | Women (n = 5) | | | *p* value (men vs. women) | | Total (n = 10) | | |
|---|---|---|---|---|---|---|---|---|---|---|---|---|
| | | C | OA | *p* value | C | OA | *p* value | C | OA | C | OA | *p* value |
| SCBP | Bone mineral density (mg/HA $cm^3$) | 602.2 ± 59.8 | 681.5 ± 58.6 | 0.022 | 591.4 ± 67.2 | 657.5 ± 48.4 | 0.018 | 0.994 | 0.938 | 596.8 ± 63.8 | 669.5 ± 55.0 | <0.001 |
| | BV/TV | 0.57 ± 0.06 | 0.67 ± 0.07 | 0.036 | 0.58 ± 0.06 | 0.67 ± 0.03 | 0.026 | 0.998 | > 0.999 | 0.57 ± 0.06 | 0.67 ± 0.05 | <0.001 |
| SCCB | Bone mineral density (mg/HA $cm^3$) | 727.4 ± 84.0 | 658.6 ± 70.2 | 0.003 | 704.3 ± 65.1 | 662.9 ± 80.0 | 0.584 | 0.977 | 0.998 | 717.1 ± 77.0 | 660.5 ± 74.8 | 0.081 |
| | BV/TV | 0.15 ± 0.03 | 0.25 ± 0.04 | 0.035 | 0.14 ± 0.02 | 0.28 ± 0.07 | 0.017 | 0.990 | 0.777 | 0.15 ± 0.03 | 0.27 ± 0.06 | <0.001 |

C, remote control sites located in the lateral tibial plateaus with grossly normal cartilage; OA, OA lesion sites in the medial tibial plateau; SCBP, subchondral bone plate; SCCB, subchondral cancellous bone; BV/TV, ratio of bone volume to tissue volume.

**Table 4. Cellular measurements in different regions of interest and between sexes.**

| | SCBP ($cells/mm^2$) | Men (n = 15) | | | Women (n = 14) | | | *p* value (men vs. women) | | Total (n = 10)# | | |
|---|---|---|---|---|---|---|---|---|---|---|---|---|
| | | C | OA | *p* value | C | OA | *p* value | C | OA | C | OA | *p* value |
| 1 | $F4/80^+$ macrophagesc | 763.2 ± 617.3* | 425.4 ± 428.2* | 0.014 | 559.6 ± 1101.3 | 385.1 ± 583.7 | 0.531 | 0.541 | 0.833 | 670.0 ± 871.5 | 406.0 ± 500.3 | 0.075 |
| 2 | $Osterix^+$ osteoprogenitors | 913.7 ± 731.5 | 930.1 ± 714.6 | 0.934 | 391.5 ± 392.4 | 475.3 ± 649.4 | 0.616 | 0.025 | 0.085 | 661.61 ± 640.0 | 710.6 ± 710.4 | 0.701 |
| 3 | Cathepsin $K^+$ osteoclasts | 380.8 ± 393.9 | 300.6 ± 244.7 | 0.172 | 407.9 ± 674.9 | 262.3 ± 269.9 | 0.377 | 0.895 | 0.692 | 393.9 ± 537.8 | 282.1 ± 253.2 | 0.177 |
| | SCCB (cells/mm) | Men (n = 18) | | | Women (n = 22) | | | *p* value (men vs. women) | | Total (n = 40)^ | | |
| | | C | OA | *p* value | C | OA | *p* value | C | OA | C | OA | *p* value |
| 1 | $F4/80^+$ | 2.3 ± 2.6* | 4.7 ± 3.3* | <0.001 | 1.6 ± 2.8 | 3.4 ± 4.5 | 0.087 | 0.447 | 0.292 | 1.9 ± 2.7* | 4.0 ± 4.0* | 0.001 |
| 2 | $Osterix^+$ | 4.5 ± 6.3 | 6.5 ± 6.4 | 0.293 | 2.5 ± 4.4 | 3.7 ± 3.7 | 0.25 | 0.248 | 0.088 | 3.4 ± 5.4 | 4.9 ± 5.2 | 0.123 |
| 3 | Cathepsin $K^+$ | 1.5 ± 1.2* | 4.4 ± 3.2* | <0.001 | 1.7 ± 3.2* | 4.9 ± 4.7* | 0.006 | 0.818 | 0.718 | 1.6 ± 2.5* | 4.7 ± 4.0* | <0.001 |

#Samples from patients X2, X3, X5, X7, X8, X9, X10, X11, X12, X15, X16, X17, and X18 contained fewer than three bone marrow cavities. Therefore, SCBP cell density data for these patients were considered nondetectable. The total number of SCBP samples included in the analysis was 29. ^Specimens from A52 (male) and X17 (male) patients retained few trabeculae under the SCBP; thus, trabecular cell density data could not be obtained for these patients. The total number of SCCB samples included in the analysis was 40. *$p < 0.05$. C, remote control sites located in the lateral tibial plateau with grossly intact cartilage; OA, OA lesion sites located in the medial tibial plateau; SCBP, subchondral bone plate; SCCB, subchondral cancellous bone.



*European Cells and Materials* Vol.56 2026 (pages 34–47) DOI: 10.22203/eCM.v056a03

other joints, such as the hip and vertebrae. For instance, a previous study observed increased BV/TV in newly formed woven bones in the SCCB of human hip OA samples [37]. A recent study on degenerative vertebral joints also compared two similar regions in the vertebral subchondral bone, namely the vertebral endplate and vertebral SCCB, and identified differences in mineral density (vertebral endplate vs. vertebral SCCB: 1.508 ± 0.107 vs. 1.93 ± 0.068 g/cm$^3$), BV/TV (vertebral endplate vs. vertebral SCCB: 0.272 ± 0.096 vs. 0.36 ± 0.13), and ash density (vertebral endplate vs. vertebral SCCB: 0.802 ± 0.173 vs. 1.01 ± 0.03 g/cm$^3$) [38]. The authors noted that their study lacked biological data to detect cellular differences between these two regions but highlighted its implications for understanding human bone remodelling [38]. In the present study, higher numbers of macrophages and osteoclasts were found in the OA SCCB, suggesting active bone remodelling in this region. Given the lower BMD observed in male donors, this activity may indicate remodelling in pathological conditions. Nevertheless, the identification of differential cell densities in the SCBP and SCCB echoes this line of inquiry and provides the first direct evidence of the detailed cellular composition of these two key regions in the OA knee (Fig. 4**g**).

Another notable finding is the difference in bone remodelling patterns between male and female patients. Female sex is a risk factor for OA. Women have a higher risk of OA due to hormonal changes and ageing [38]. Oestrogen, the primary sex hormone regulating bone mass, acts mainly through oestrogen receptor-$\alpha$ (ER$\alpha$) [40]. A recent animal study revealed that osteoclastic ER$\alpha$ is crucial for maintaining the trabecular bone in female mice but is dispensable in male mice [41]. Clinical data also indicate that women with hip OA are more susceptible to polyarticular OA and tend to experience greater symptomatic and structural severity than men [42]. In the present study, bone remodelling properties of the SCBP and SCCB regions differed between postmenopausal women and men (Table 4, Figs.2 and 3). Fewer osteoprogenitor cells were found in the control SCBP in female donors than male donors (Table 4, female vs. male: 391.5 ± 392.4 vs. 913.7 ± 731.5, $p$ = 0.025), demonstrating one aspect of the potential sex-related difference in SCBP remodelling. Recently, Hayes *et al.* [43] reported that bisphosphonates (e.g., alendronate and risedronate) might be more protective against early knee OA (KL grade <2) in female patients, particularly among those with are not overweight (BMI <25 kg/m$^2$) but less protective among patients with more advanced disease (KL grade ≥ 2) or in those who are overweight (BMI ≥ kg/m$^2$). In the present study, female patients had a 7% higher density of CTSK$^+$ osteoclasts than did male patients in the SCBP C region (Table 4, female vs. male: 407.9 ± 674.9 vs. 380.8 ± 393.9 cells/mm$^2$). These subtle cellular differences may partially explain the greater protective effects of bone-activating reagents in women with early knee OA because a higher number of responsive cells in the subchondral bone could enhance the efficacy of such treatments. This finding also suggests that the subchondral bone can be a potential therapeutic target for bone-activating reagents in OA. Møller *et al.* [44] investigated the osteoclastogenic capacity of CD14$^+$ blood monocytes isolated from 49 female donors (mean age: 53 years; premenopausal: 17 donors; postmenopausal: 32 donors) and found that the protein level of CTSK was significantly higher in monocyte-derived osteoclasts from postmenopausal donors than in those from premenopausal donors (more than double, $p$ = 0.0158, [44]). This may also provide a plausible explanation for the higher level of CTSK$^+$ cells found in the present study. Regarding the sex-related difference observed in the current study, sex hormones are likely to modulate these load-driven programmes. Oestrogen/ER$\alpha$ [45] restrains osteoclastogenesis and supports osteogenesis, which may help to preserve the positive coupling between F4/80$^+$ macrophages and Osterix$^+$ osteoprogenitors across regions in women (Fig.4**c–f**). By contrast, varus malalignment–induced overload and SCBP sclerosis [29] may preferentially disrupt this coupling in male OA samples, consistent with the attenuated correlation observed in male OA (Fig.4**d**, 4**f**).

In the present study, all specimens were obtained from patients with OA who had knee varus deformity, and the control sites were located in the lateral compartment. Although the control regions did not represent completely healthy osteochondral tissue, both control and OA regions were obtained from the same chronically inflamed joint cavity. The mechanical loading in the lateral compartment (control region) was lower than that in the medial compartment (OA region). Thus, the parameters measured here are likely to reflect the combined effects of chronic altered loading and inflammation on subchondral bone cells. For example, the findings demonstrated that in both male and female subchondral cancellous bone, the number of CTSK$^+$ osteoclasts was significantly higher in the load-bearing OA region than in the control region, suggesting that excessive mechanical loading enhances osteoclastogenesis. This observation is consistent with that of a previous animal study reporting increased osteoclast numbers in overloaded maxillary molars [24]. CTSK$^+$ osteoclasts were also prevalent in OA SCCB tissues from both sexes (Fig.3**d**, 3**i**), although no significant differences in osteoclast counts were detected between OA and control regions in the SCBP. These results indicate that even in end-stage OA, the subchondral cancellous bone may continue to undergo active remodelling beneath the sclerotic SCBP. In addition, the significantly higher numbers of F4/80$^+$ macrophages in the SCBP control sites compared with OA regions in male patients (Fig.2**b**–**h**) indicate that macrophages are mechanoresponsive, and excessive mechanical loading in OA regions may inhibit F4/80$^+$ macrophage activity and the associ-

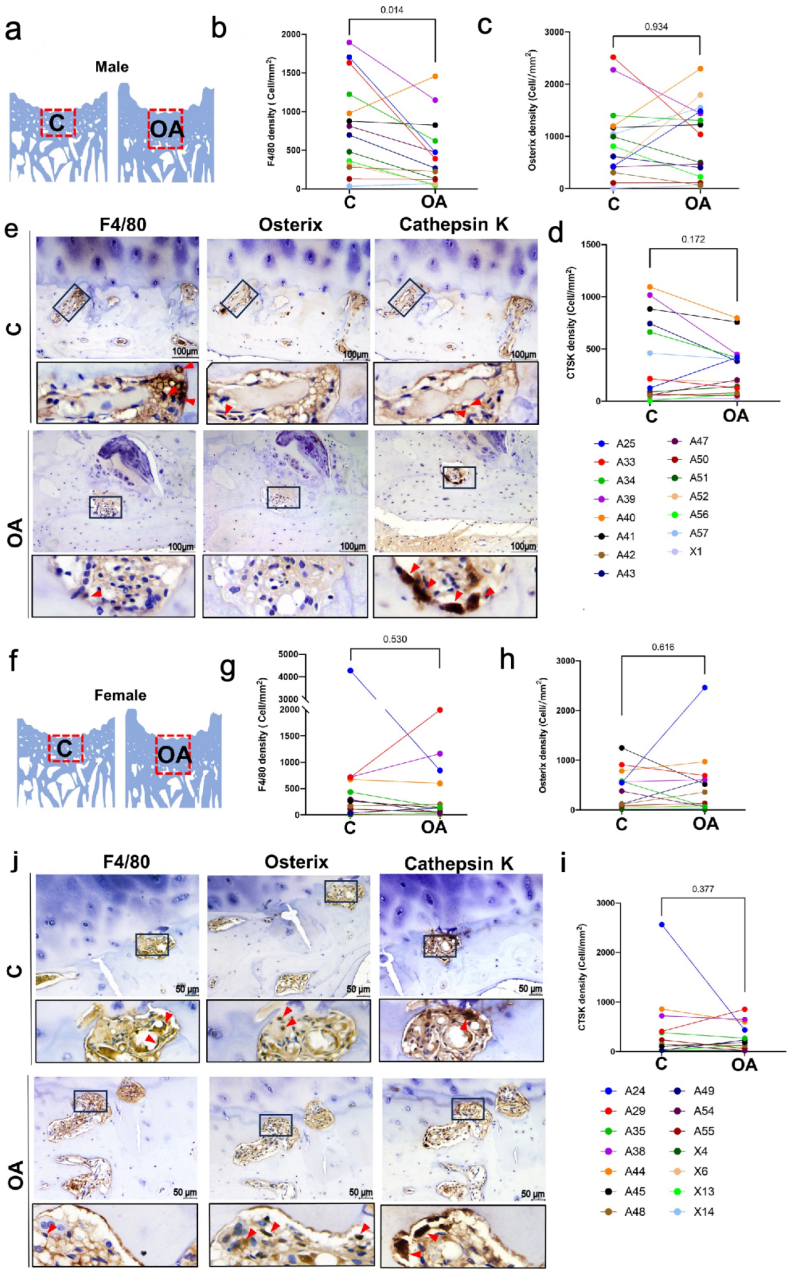


**Fig. 2. Cellular density and distribution of macrophages, osteoprogenitors, and osteoclasts in SCBP regions.** (**a**) Schematic diagram of the SCBP region in male patients; red box: ROI. (**b—d**) Density of F4/80$^+$ macrophages (**b**), Osterix$^+$ osteoprogenitor cells (**c**), and CTSK$^+$ osteoclasts (**d**) in bone marrow cavities of the SCBP in male patients. The Wilcoxon signed-rank test was used to compare data between the C and OA regions; n = 15 men. Data are presented as the mean ± SD, *$p < 0.05$. (**f**) Schematic diagram of the SCBP region in female patients; red box: ROI. (**g—i**) Density of F4/80+ macrophages (g), Osterix+ osteoprogenitor cells (**h**), and CTSK$^+$ osteoclasts (**i**) in the SCBP of female patients. The Wilcoxon signed-rank test was used to compare data between the C and OA regions; n = 14 women. Data are presented as the mean ± SD, *$p < 0.05$. Representative sequential IHC staining of F4/80, Osterix, and cathepsin K in SCBP bone marrow cavities from male (**e**) and female (**j**) patients. Upper panel: control sites; lower panel: OA regions. The rectangular black box shows the magnified field of the upper image. Samples with fewer than three bone marrow cavities did not provide detectable data and therefore were excluded from quantification. Red arrowheads indicate positive staining signals: F4/80 (mainly in the cytoplasm and extracellular matrix), Osterix (mainly in the nucleus), and cathepsin K (mainly in the cytoplasm and nucleus). The scale bar represents 100 μm in (**e**). The scale bar represents 50 μm in (**j**). C, remote control sites located in the lateral tibial plateaus with grossly normal cartilage; OA, OA lesion sites in the medial tibial plateaus; SCBP, subchondral bone plate; ROI: region of interest; CTSK, cathepsin K.

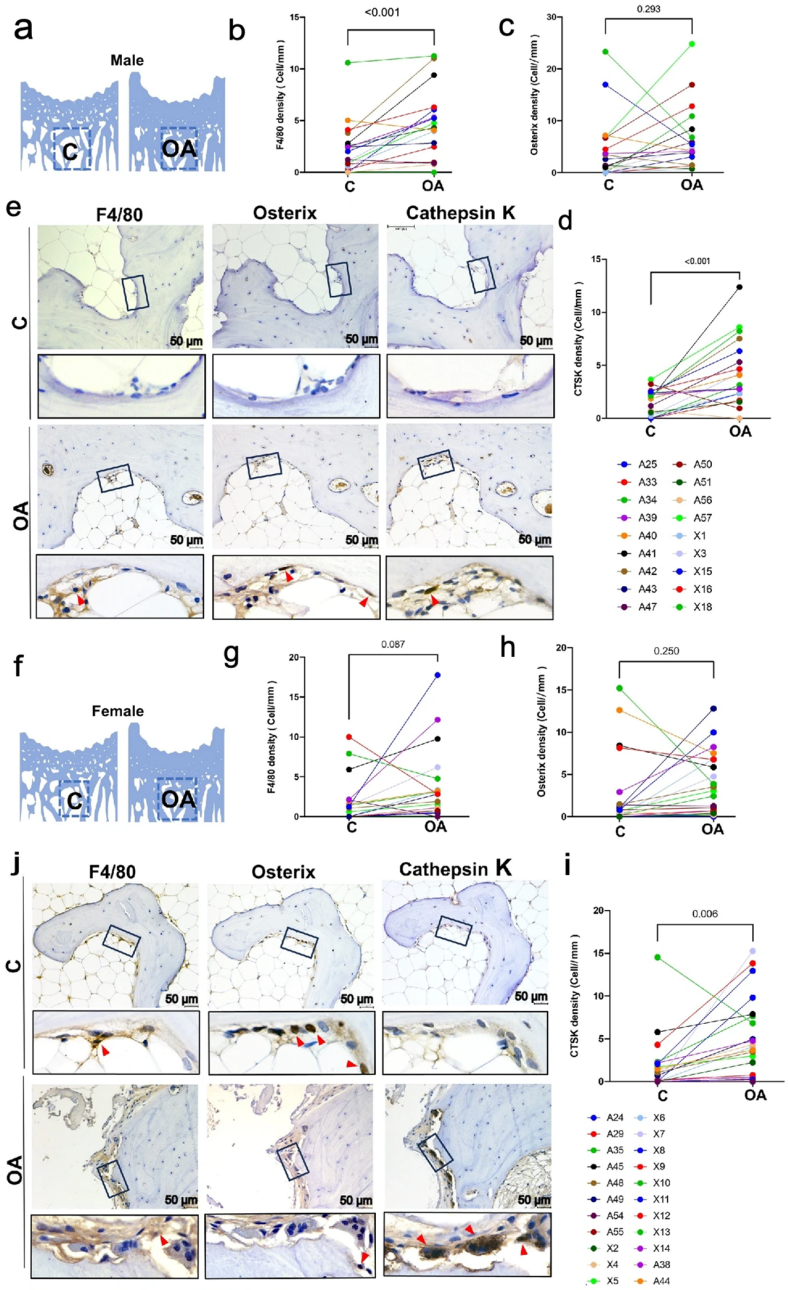


**Fig. 3. Cellular density and distribution of macrophages, osteoprogenitors, and osteoclasts in SCCB regions.** (**a**) Schematic diagram of the SCCB region in male patients; blue box: ROI. (**b–d**) Density of F4/80$^+$ macrophages (**b**), Osterix$^+$ osteoprogenitor cells (**c**), and CTSK$^+$ osteoclasts (**d**) in the bone marrow cavities of the SCCB in male patients. The Wilcoxon signed-rank test was used to compare data between the C and OA regions; n = 18 men. Data are presented as the mean ± SD, *$p < 0.05$. (**f**) Schematic diagram of the SCCB region in female patients; blue box: ROI. (**g–i**) Density of F4/80$^+$ macrophages (**g**), Osterix$^+$ osteoprogenitor cells (**h**), and CTSK$^+$ osteoclasts (**i**) in the SCBP region in female patients. The Wilcoxon signed-rank test was used to compare data between the C and OA regions; n = 22 women. Data are presented as the mean ± SD, *$p < 0.05$. Representative sequential IHC staining of F4/80, Osterix, and cathepsin K in SCCB bone surfaces from male (**e**) and female (**j**) patients. The scale bar represents 50 $\mu$m in (e) and (j). Upper panel: control sites; lower panel: OA regions. The rectangular black box shows the magnified field of the upper image. Samples with fewer than three bone marrow cavities did not provide detectable data and were therefore excluded from quantification. Red arrowheads indicate positive staining signals: F4/80 (mainly in the cytoplasm and extracellular matrix), Osterix (mainly in the nucleus), and Cathepsin K (mainly in the cytoplasm and nucleus).

C, remote control sites located in the lateral tibial plateaus with grossly normal cartilage; OA, OA lesion sites in the medial tibial plateaus; SCCB, subchondral cancellous bone; ROI, region of interest; CTSK, Cathepsin K.

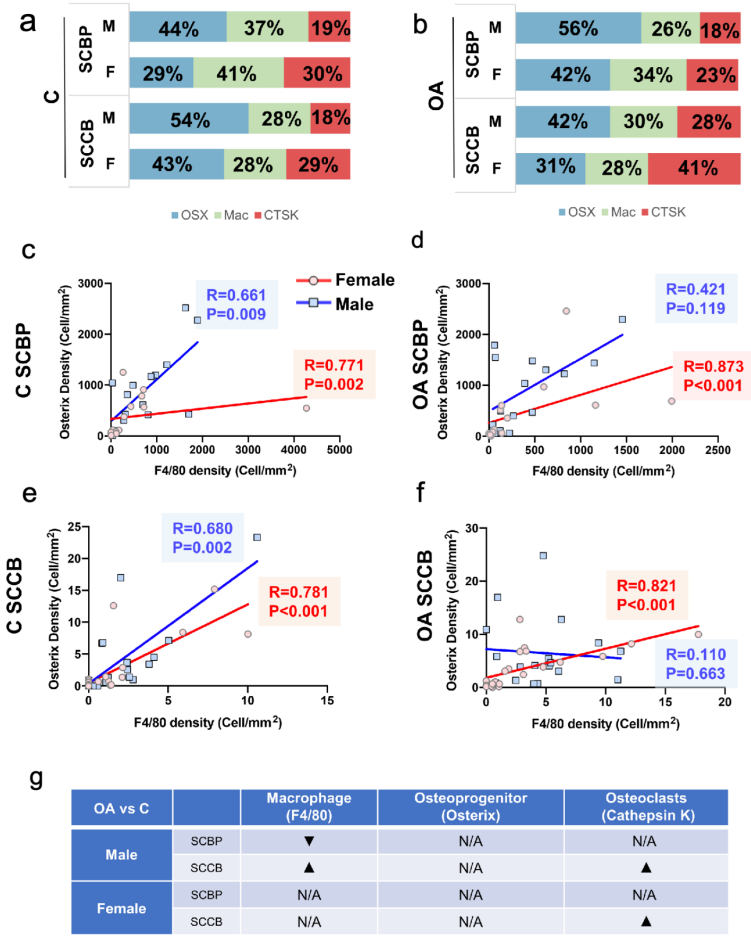


g

| OA vs C | | Macrophage (F4/80) | Osteoprogenitor (Osterix) | Osteoclasts (Cathepsin K) |
|---|---|---|---|---|
| Male | SCBP | ▼ | N/A | N/A |
| | SCCB | ▲ | N/A | ▲ |
| Female | SCBP | N/A | N/A | N/A |
| | SCCB | N/A | N/A | ▲ |

**Fig. 4. Cellular components and their correlations in different regions of the OA subchondral bone.** (**a, b**) Proportion of cellular components in the C region (**a**) and OA region (**b**). Bars show the numbers of Osterix$^+$ osteoprogenitors (in blue), F4/80$^+$ macrophages (in green), and CTSK$^+$ osteoclasts (in red) in the SCBP and SCCB regions of male and female donors. (**c–f**). Correlation analysis between F4/80$^+$ macrophages and Osterix$^+$ osteoprogenitors in the SCBP and SCCB of both C and OA regions. Data from female patients are shown in red, and data from male patients are shown in blue. Spearman's rank correlation was used to determine associations based on immunohistochemistry quantification data, and the correlation coefficient r and *p* values are listed in each figure. (**g**) Summary of cellular changes noted in different regions and sexes. Black upward arrowheads indicate increases, whereas black downward arrowheads indicate reductions.

C, remote control sites located in the lateral tibial plateaus with grossly normal cartilage; OA, OA lesion sites in the medial tibial plateaus; SCBP, subchondral bone plate; SCCB, subchondral cancellous bone; ROI, region of interest; CTSK, cathepsin K.

ated physiological mineralisation. A recent study identified several mechanoresponsive signalling pathways involved in bone remodelling, including Piezo1/YAP/TAZ [46], Transforming Growth Factor-$\beta$ signalling [47–49], and Sirt3/E11/gp38 [50]. Thus, therapeutic strategies targeting these mechanosensitive pathways in the subchondral bone [51] are worthy of further investigation.

There are, however, limitations of this study. Firstly, the use of naturally collected clinical samples inevitably introduced variability in sample quality, resulting in higher overall data variability. The sample size in this study is still relatively small. Secondly, approximately one third of patients had a history of taking statin-related drugs such as simvastatin and rosuvastatin. Because statin administration can affect bone metabolism [52], data from these patients may have been influenced by their underlying health conditions and medication use. Accordingly, we analysed the current data set on the effects of statins (**Supplementary Material Table 6**), and this information is for reference only because only 8 patients in this cohort used statins. More sample number is needed in the near future to confirm this observation. Moreover, when linear mixed models were used to examine and account for potential confounding factors, such as BMI, age, hypertension, and diabetes mellitus, it was found that these factors did not affect the statistical outcomes of the cellular data (**Supplementary**

**Material Table 7**). A third limitation of this study is that most conclusions are based on bone histomorphometric measurements. Cell densities in the SCBP were not compared with those in the SCCB due to differences in basal cellular numbers and calculation methods [53]. Additionally, it is technically challenging to completely exclude underlying cancellous tissue when quantifying the SCBP in $\mu$CT analyses [54]. Finally, the control sites in this study did not represent truly normal tissue because they were collected from OA knees. After all, obtaining subchondral bone tissues from healthy donors remains a major challenge. The subchondral bone in these control sites was also subjected to chronic altered loading and inflammatory events. Thus, the results of the control group cannot fully represent normal, non-inflammatory subchondral bone remodelling under physiological loading conditions. Further investigations using the subchondral bone from healthy donors are therefore warranted. Ideally, future studies should obtain control osteochondral samples from anatomically paired zones adjacent to the medial site in both OA and healthy joints to avoid variations in structural and cell parameters between sites.

## Conclusions

Region-specific differences in cellular components were identified in the OA subchondral bone, particularly among tissue-resident macrophages and osteoclasts in the SCBP and SCCB regions. This study revealed the enrichment of F4/80$^+$ resident macrophages in the male control (non-injury) SCBP and cathepsin K$^+$ osteoclasts in the OA (load-bearing) SCCB of both male and female patients. These findings reflect the combined effects of chronic altered loading and inflammation on cellular activity across different regions of the OA subchondral bone and provide new insights into the pathophysiological mechanisms underlying OA.

## List of Abbreviations

3D, Three-dimensional; ACL, anterior cruciate ligament; BMI, body mass index; BMD, bone mineral density; BV/TV, bone volume to tissue volume ratio; C (region), control region; CD14, cluster of differentiation 14; CD68, cluster of differentiation 68; CD169, cluster of differentiation 169; CTSK, cathepsin K; ER$\alpha$, oestrogen receptor alpha; F4/80, F4/80 antigen (bone resident macrophage marker); HKA, hip–knee–ankle angle; KL, kellgren–Lawrence (radiographic grading); MRI, magnetic resonance imaging; MPTA, medial proximal tibial angle; OA, osteoarthritis; OARSI, osteoarthritis Research Society International; OSM, Osteoarthritis M; ROI, region of interest; SCBP, subchondral bone plate; SCCB, subchondral cancellous bone; SDF 1, stromal cell derived factor 1; Sirt3, sirtuin 3; STAT3, signal transducer and activator of transcription 3; TAZ, transcriptional coactivator with PDZ binding motif; TGF-$\beta$, transforming growth factor $\beta$; YAP / YAP1, yes associated protein / yes associated protein 1; $\mu$CT, micro computed tomography.

## Availability of Data and Materials

All data that support the findings of this study are available online, as shown in the supplementary data. The detailed original raw data are available from the corresponding author upon reasonable request.

## Author Contributions

XBZ: Conceptualization, Investigation, data collection, visualization, validation, methodology, formal analysis, original draft of the manuscript; MDC: data collection, visualization, validation, methodology, formal analysis; CH, WQX: data collection, validation, methodology; ZYX data validation, writing—review & editing; KKWH, MTYO, WFX, PSHY and YSL: supervision, resources, methodology, and provided patient samples for this work; YSL, CJL, and YZJ: supervision, funding acquisition; YZJ: Writing—review & editing, Writing—original draft, Visualization, Validation, Supervision, Resources, Project administration, Methodology, Investigation, Funding acquisition, Formal analysis, Data Curation, Conceptualization. All authors read and approved the final manuscript. All authors agree to be accountable for all aspects of the work in ensuring that questions related to the accuracy or integrity of any part of the work are appropriately investigated and resolved. No AI and AI-assisted technologies were used in the writing process.

## Ethics Approval and Consent to Participate

The research protocol was approved by the Human Research Ethics Committees of local Administrative Parties (NTEC/CREC Ref. 2013.248 and 2019.078; IRB of Xiangya Hospital: Ref. 202004147). Informed consent was obtained from all subjects.

## Acknowledgment

All authors appreciated the technical support from the core facilities in the School of Biomedical Science and the Department of Orthopaedics and Traumatology. We would like to specifically thank Miss. Stacy Yam Lok Sze, Miss. Queena Poon Wai Chin, and Miss. Helen Chan Yau Tsz for their assistance in collecting clinical specimens, and Dr. Bruma Fu Sai Chuen for the suggestions on data analysis. We sincerely thank all the supports from all parties during the COVID-19 pandemic.

## Funding

This work was supported by (i) the National Key R&D Program of China (project number 2019YFA0111900 to YJ, CL, YL), which is financed by the Ministry of Science and Technology of the People's Republic of China (MOST, China); (ii) NSFC/RGC Joint Research Scheme

sponsored by the Research Grants Council of the Hong Kong SAR, China and the National Natural Science Foundation of China (Project No. N_CUHK483/22); (iii) NSFC (Project No. 8221101064 to CL); (iv) the Center for Neuromusculoskeletal Restorative Medicine [CNRM at InnoHK, to YJ, PY] by Innovation and Technology Commission (ITC) of Hong Kong SAR, China.

## Conflict of Interest

The authors declare no conflict of interest.

## Supplementary Material

Supplementary material associated with this article can be found, in the online version, at https://??.

## References

[1] Hu W, Chen Y, Dou C, Dong S. Microenvironment in subchondral bone: predominant regulator for the treatment of osteoarthritis. Annals of the Rheumatic Diseases. 2021; 80: 413–422. https://doi.org/10.1136/annrheumdis-2020-218089.

[2] Zhu X, Chan YT, Yung PSH, Tuan RS, Jiang Y. Subchondral bone remodeling: A therapeutic target for osteoarthritis. Frontiers in Cell and Developmental Biology. 2021; 8: 607764. https://doi.org/10.3389/fcell.2020.607764.

[3] Gimarc DC, Jesse Lowry MK. Bone marrow signal abnormalities in arthritis and trauma. Journal of Cartilage & Amp; Joint Preservation. 2024; 4: 100157. https://doi.org/10.1016/j.jcjp.2023.100157.

[4] Khokhar K, Conaghan PG. Bone in osteoarthritis: imaging and interventions. Current Opinion in Rheumatology. 2022; 34: 73–78. https://doi.org/10.1097/bor.0000000000000849.

[5] Lee Y, Findlay DM, Muratovic D, Kuliwaba JS. Greater heterogeneity of the bone mineralisation density distribution and low bone matrix mineralisation characterise tibial subchondral bone marrow lesions in knee osteoarthritis patients. Bone. 2021; 149: 115979. https://doi.org/10.1016/j.bone.2021.115979.

[6] Donell S. Subchondral bone remodelling in osteoarthritis. EFORT Open Reviews. 2019; 4: 221–229. https://doi.org/10.1302/2058-5241.4.180102.

[7] Wang LJ, Zeng N, Yan ZP, Li JT, Ni GX. Post-traumatic osteoarthritis following ACL injury. Arthritis Research & Amp; Therapy. 2020; 22: 57. https://doi.org/10.1186/s13075-020-02156-5.

[8] Bhatla JL, Kroker A, Manske SL, Emery CA, Boyd SK. Differences in subchondral bone plate and cartilage thickness between women with anterior cruciate ligament reconstructions and uninjured controls. Osteoarthritis and Cartilage. 2018; 26: 929–939. https://doi.org/10.1016/j.joca.2018.04.006.

[9] Kroker A, Bhatla JL, Emery CA, Manske SL, Boyd SK. Subchondral bone microarchitecture in ACL reconstructed knees of young women: a comparison with contralateral and uninjured control knees. Bone. 2018; 111: 1–8. https://doi.org/10.1016/j.bone.2018.03.006.

[10] Bolbos RI, Zuo J, Banerjee S, Link TM, Benjamin Ma C, Li X, *et al*. Relationship between trabecular bone structure and articular cartilage morphology and relaxation times in early OA of the knee joint using parallel MRI at 3 T. Osteoarthritis and Cartilage. 2008; 16: 1150–1159. https://doi.org/10.1016/j.joca.2008.02.018.

[11] Li Y, Liem Y, Dall'Ara E, Sullivan N, Ahmed H, Blom A, *et al*. Subchondral bone microarchitecture and mineral density in human osteoarthritis and osteoporosis: a regional and compartmental analysis. Journal of Orthopaedic Research. 2021; 39: 2568–2580. https://doi.org/10.1002/jor.25018.

[12] Chen Y, Hu Y, Yu YE, Zhang X, Watts T, Zhou B, *et al*. Subchondral Trabecular Rod Loss and Plate Thickening in the Development of Osteoarthritis. Journal of Bone and Mineral Research. 2018; 33: 316–327. https://doi.org/10.1002/jbmr.3313.

[13] Zhen G, Wen C, Jia X, Li Y, Crane JL, Mears SC, *et al*. Inhibition of TGF-$\beta$ signaling in mesenchymal stem cells of subchondral bone attenuates osteoarthritis. Nature Medicine. 2013; 19: 704–712. https://doi.org/10.1038/nm.3143.

[14] Zhou F, Han X, Wang L, Zhang W, Cui J, He Z, *et al*. Associations of osteoclastogenesis and nerve growth in subchondral bone marrow lesions with clinical symptoms in knee osteoarthritis. Journal of Orthopaedic Translation. 2022; 32: 69–76. https://doi.org/10.1172/jci121561.

[15] Zhu S, Zhu J, Zhen G, Hu Y, An S, Li Y, *et al*. Subchondral bone osteoclasts induce sensory innervation and osteoarthritis pain. The Journal of Clinical Investigation. 2019; 129: 1076–1093. https://doi.org/10.1172/jci121561.

[16] Ding R, Zhang N, Wang Q, Wang W. Alterations of the subchondral bone in osteoarthritis: Complying with Wolff's Law. Current Rheumatology Reviews. 2022; 18: 178–185. https://doi.org/10.2174/1573397118666220401104428.

[17] Cui Z, Crane J, Xie H, Jin X, Zhen G, Li C, *et al*. Halofuginone attenuates osteoarthritis by inhibition of TGF-$\beta$ activity and H-type vessel formation in subchondral bone. Annals of the Rheumatic Diseases. 2016; 75: 1714–1721. https://doi.org/10.1136/annrheumdis-2015-207923.

[18] Chang MK, Raggatt LJ, Alexander KA, Kuliwaba JS, Fazzalari NL, Schroder K, *et al*. Osteal Tissue Macrophages are Intercalated throughout Human and Mouse Bone Lining Tissues and Regulate Osteoblast Function in Vitro and in Vivo. the Journal of Immunology. 2008; 181: 1232–1244. https://doi.org/10.4049/jimmunol.181.2.1232.

[19] Batoon L, Millard SM, Wullschleger ME, Preda C, Wu AC, Kaur S, *et al*. CD169$^+$ macrophages are critical for osteoblast maintenance and promote intramembranous and endochondral ossification during bone repair. Biomaterials. 2019; 196: 51–66. https://doi.org/10.1016/j.biomaterials.2017.10.033.

[20] Wang J, Zheng Z, Huang B, Wu H, Zhang X, Chen Y, *et al*. Osteal Tissue Macrophages are Involved in Endplate Osteosclerosis through the OSM-STAT3YAP1 Signaling Axis in Modic Changes. the Journal of Immunology. 2020; 205: 968–980. https://doi.org/10.4049/jimmunol.1901001.

[21] Batoon L, Millard SM, Raggatt LJ, Wu AC, Kaur S, Sun LWH, *et al*. Osteal macrophages support osteoclast-mediated resorption and contribute to bone pathology in a postmenopausal osteoporosis mouse model. Journal of Bone and Mineral Research: the official journal of the American Society for Bone and Mineral Research. 2021; 36: 2214–2228. https://doi.org/10.1002/jbmr.4413.

[22] Dong L, Song Y, Zhang Y, Zhao W, Wang C, Lin H, *et al*. Mechanical stretch induces osteogenesis through the alternative activation of macrophages. Journal of Cellular Physiology. 2021; 236: 6376–6390. https://doi.org/10.1002/jcp.30312.

[23] Deng R, Li C, Wang X, Chang L, Ni S, Zhang W, et al. Periosteal CD68$^+$ F4/80$^+$ macrophages are mechanosensitive for cortical bone formation by secretion and activation of TGF-$\beta$1. Advanced Science. 2022; 9: e2103343. https://doi.org/10.1002/advs.202103343.

[24] Nozaki K, Kaku M, Yamashita Y, Yamauchi M, Miura H. Effect of cyclic mechanical loading on osteoclast recruitment in periodontal tissue. Journal of Periodontal Research. 2010; 45: 8–15. https://doi.org/10.1111/j.1600-0765.2008.01193.x.

[25] Wang X, Ji L, Wang J, Liu C. Matrix stiffness regulates osteoclast fate through integrin-dependent mechanotransduction. Bioactive Materials. 2023; 27: 138–153. https://doi.org/10.1016/j.bioactmat.2023.03.014.

[26] Bertuglia A, Lacourt M, Girard C, Beauchamp G, Richard H, Laverty S. Osteoclasts are recruited to the subchondral bone in naturally occurring post-traumatic equine carpal osteoarthritis and may con-

tribute to cartilage degradation. Osteoarthritis and Cartilage. 2016; 24: 555–566. https://doi.org/10.1016/j.joca.2015.10.008.

[27] Colyn W, Azari F, Bellemans J, Harry van Lenthe G, Scheys L. Microstructural adaptations of the subchondral bone are related to the mechanical axis deviation in end stage varus OA knees. European Cells and Materials. 2023; 45: 60–71. https://doi.org/10.22203/ecm.v045a05.

[28] Zeng ZJ, PengPeng, Huang CL, Yao F, Wu J, Gu B, *et al*. More severe microdamage and micromechanical alterations: altered subchondral bone remodeling in varus knee osteoarthritis with osteoporosis. Osteoporosis International. 2025; 36: 2483–2495. https://doi.org/10.1007/s00198-025-07652-5.

[29] Geurts J, Patel A, Hirschmann MT, Pagenstert GI, Müller-Gerbl M, Valderrabano V, *et al*. Elevated marrow inflammatory cells and osteoclasts in subchondral osteosclerosis in human knee osteoarthritis. Journal of Orthopaedic Research. 2016; 34: 262–269. https://doi.org/10.1002/jor.23009.

[30] Segal NA, Nilges JM, Oo WM. Sex differences in osteoarthritis prevalence, pain perception, physical function and therapeutics. Osteoarthritis and Cartilage. 2024; 32: 1045–1053. https://doi.org/10.1016/j.joca.2024.04.002.

[31] Atasoy-Zeybek A, Showel KK, Nagelli CV, Westendorf JJ, Evans CH. The intersection of aging and estrogen in osteoarthritis. NPJ Womens Health. 2025; 3:15. https://doi.org/10.1038/s44294-025-00063-1.

[32] Pang H, Chen S, Klyne DM, Harrich D, Ding W, Yang S, *et al*. Low back pain and osteoarthritis pain: a perspective of estrogen. Bone Research. 2023; 11: 42. https://doi.org/10.1038/s41413-023-00280-x.

[33] Ogawa H, Nakamura Y, Sengoku M, Shimokawa T, Sohmiya K, Ohnishi K, *et al*. Medial proximal tibial angle at the posterior tibial plateau represents the pre-arthritic constitutional medial proximal tibial angle in anterior cruciate ligament-intact, advanced osteoarthritis of the knee. Knee Surgery, Sports Traumatology, Arthroscopy. 2022; 30: 2941–2947. https://doi.org/10.1007/s00167-022-06890-y.

[34] Nagira K, Ikuta Y, Shinohara M, Sanada Y, Omoto T, Kanaya H, *et al*. Histological scoring system for subchondral bone changes in murine models of joint aging and osteoarthritis. Scientific Reports. 2020; 10: 10077. https://doi.org/10.1038/s41598-020-66979-7.

[35] Pritzker KPH, Gay S, Jimenez SA, Ostergaard K, Pelletier J-P, Revell PA, *et al*. Osteoarthritis cartilage histopathology: grading and staging. Osteoarthritis and Cartilage. 2006; 14: 13–29. https://doi.org/10.1016/j.joca.2005.07.014.

[36] Hong Q, Liu ZX, Liang HF, Wu DG, Chen Y, Yu B. Inhibition of HOXD11 promotes cartilage degradation and induces osteoarthritis development. Journal of Orthopaedic Surgery and Research. 2024; 19: 111. https://doi.org/10.1186/s13018-024-04573-7.

[37] Boyde A. The Bone Cartilage Interface and Osteoarthritis. Calcified Tissue International. 2021; 109: 303–328. https://doi.org/10.1007/s00223-021-00866-9.

[38] Wu Y, Loaiza J, Banerji R, Blouin O, Morgan E. Structure-function relationships of the human vertebral endplate. JOR Spine. 2021; 4: e1170. https://doi.org/10.1002/jsp2.1170.

[39] Boyan BD, Tosi LL, Coutts RD, Enoka RM, Hart DA, Nicolella DP, *et al*. Addressing the gaps: sex differences in osteoarthritis of the knee. Biology of Sex Differences. 2013; 4: 4. https://doi.org/10.1186/2042-6410-4-4.

[40] Zhou R, Guo Q, Xiao Y, Guo Q, Huang Y, Li C, et al. Endocrine role of bone in the regulation of energy metabolism. Bone Research. 2021; 9: 25. https://doi.org/10.1038/s41413-021-00142-4.

[41] Nakamura T, Imai Y, Matsumoto T, Sato S, Takeuchi K, Igarashi K, *et al*. Estrogen Prevents Bone Loss via Estrogen Receptor $\alpha$ and Induction of Fas Ligand in Osteoclasts. Cell. 2007; 130: 811–823. https://doi.org/10.1016/j.cell.2007.07.025.

[42] Maillefert JF, Gueguen A, Monreal M, Nguyen M, Berdah L, Lequesne M, *et al*. Sex differences in hip osteoarthritis: results of a longitudinal study in 508 patients. Annals of the Rheumatic Diseases. 2003; 62: 931–934. https://doi.org/10.1136/ard.62.10.931.

[43] Hayes KN, Giannakeas V, Wong AKO. Bisphosphonate Use is Protective of Radiographic Knee Osteoarthritis Progression among those with Low Disease Severity and being Non-Overweight: Data from the Osteoarthritis Initiative. Journal of bone and mineral research : the official journal of the American Society for Bone and Mineral Research. 2020; 35: 2318–2326. https://doi.org/10.1002/jbmr.4133.

[44] Møller AMJ, Delaissé JM, Olesen JB, Madsen JS, Canto LM, Bechmann T, *et al*. Aging and menopause reprogram osteoclast precursors for aggressive bone resorption. Bone Research. 2020; 8: 27. https://doi.org/10.1038/s41413-020-0102-7.

[45] Kim HN, Ponte F, Nookaew I, Ucer Ozgurel S, Marques-Carvalho A, Iyer S, *et al*. Estrogens decrease osteoclast number by attenuating mitochondria oxidative phosphorylation and ATP production in early osteoclast precursors. Scientific Reports. 2020; 10: 11933. https://doi.org/10.1038/s41598-020-68890-7.

[46] Wang L, You X, Lotinun S, Zhang L, Wu N, Zou W. Mechanical sensing protein PIEZO1 regulates bone homeostasis via osteoblast-osteoclast crosstalk. Nature Communications. 2020; 11: 282. https://doi.org/10.1038/s41467-019-14146-6.

[47] Bailey KN, Nguyen J, Yee CS, Dole NS, Dang A, Alliston T. Mechanosensitive Control of Articular Cartilage and Subchondral Bone Homeostasis in Mice Requires Osteocytic Transforming Growth Factor $\beta$ Signaling. Arthritis & rheumatology. 2021; 73: 414–425. https://doi.org/10.1002/art.41548.

[48] Mazur CM, Woo JJ, Yee CS, Fields AJ, Acevedo C, Bailey KN, *et al*. Osteocyte dysfunction promotes osteoarthritis through MMP13-dependent suppression of subchondral bone homeostasis. Bone Research. 2019; 7: 34. https://doi.org/10.1038/s41413-019-0070-y .

[49] Zhen G, Guo Q, Li Y, Wu C, Zhu S, Wang R, *et al*. Mechanical stress determines the configuration of TGF$\beta$ activation in articular cartilage. Nature Communications. 2021; 12: 1706. https://doi.org/10.1038/s41467-021-21948-0.

[50] Li Q, Wang R, Zhang Z, Wang H, Lu X, Zhang J, *et al*. Sirt3 mediates the benefits of exercise on bone in aged mice. Cell death and differentiation. 2023; 30: 152–167. https://doi.org/10.1038/s41418-022-01053-5.

[51] Zhu X, Cao M, Li K, Chan Y, Chan H, Mak Y, *et al*. Intra-articular sustained-release of pirfenidone as a disease-modifying treatment for early osteoarthritis. Bioactive Materials. 2024; 39: 255–272. https://doi.org/10.1016/j.bioactmat.2024.05.028.

[52] Garrett IR, Mundy GR. The role of statins as potential targets for bone formation. Arthritis Research. 2002; 4: 237–240. https://doi.org/10.1186/ar413.

[53] Chamani S, Liberale L, Mobasheri L, Montecucco F, Al-Rasadi K, Jamialahmadi T, *et al*. The role of statins in the differentiation and function of bone cells. European Journal of Clinical Investigation. 2021; 51: e13534. https://doi.org/10.1111/eci.13534.

[54] Harrigan TP, Jasty M, Mann RW, Harris WH. Limitations of the continuum assumption in cancellous bone. Journal of Biomechanics. 1988; 21: 269–275. https://doi.org/10.1016/0021-9290(88)90257-6.

**Editor's note**: The Scientific Editor responsible for this paper was Laura Creemers and Martin Stoddart.

**Received**: 3rd June 2025; **Accepted**: 27th January 2026; **Published**: 30th April 2026